I&EC research
Industrial & Engineering Chemistry Research
pubs.acs.org/IECR
Article

Controllable Synthesis of Hollow Mesoporous ZSM-5 with Improved Catalytic Performance for Tetralin Hydrocracking to Light Aromatics

Haoqing Zhang,[‖] Limin Zhang,[‖] Mengdi Wang, Keyan Li,* Anfeng Zhang, Hao Wang, Jiaming Wu, Shanfan Lin, Duo Li, Chunshan Song, and Xinwen Guo*

Cite This: *Ind. Eng. Chem. Res.* 2025, 64, 4330−4341

ABSTRACT: Traditional ZSM-5 zeolite with a microporous structure suffers from diffusion limitations for large molecules and poor accessibility to active centers, resulting in low catalytic activity and rapid deactivation via coking. Herein, we designed and prepared ZSM-5 with hollow cavity and uniform mesopores in the shell through one-step alkali treatment using mixed alkali of tetrapropylammonium hydroxide (TPAOH) and sodium carbonate (Na_2CO_3). The size of mesopores in the shell could be controlled in the range of 2−12 nm by simply changing the concentration of Na_2CO_3. The effects of alkali treatment time, Si/Al ratio of parent ZSM-5, and zeolite/solution ratio on the formation of mesopores were systematically investigated. The construction of hollow mesoporous structure for ZSM-5 led to a significant improvement of catalytic activity in the conversion of tetralin to benzene, toluene, ethylbenzene, and xylene (BTEX). The tetralin conversion and BTEX yield for hollow mesoporous ZSM-5 achieved 99.6% and 49.2%, respectively, while those of solid ZSM-5 were 94.0% and 41.6%, respectively. Moreover, the lifespan of hollow mesoporous ZSM-5 was significantly prolonged compared with solid ZSM-5. The enhanced catalytic performance of hollow mesoporous ZSM-5 could be attributed to reduced diffusional resistance and increased accessibility to acid sites as well as improved tolerance capacity of coke species. This study provides a facile and effective strategy for the preparation of zeolite catalysts with uniform and tunable mesopores and also exhibits the advantages of mesoporous zeolites in the reactions related to large molecules.

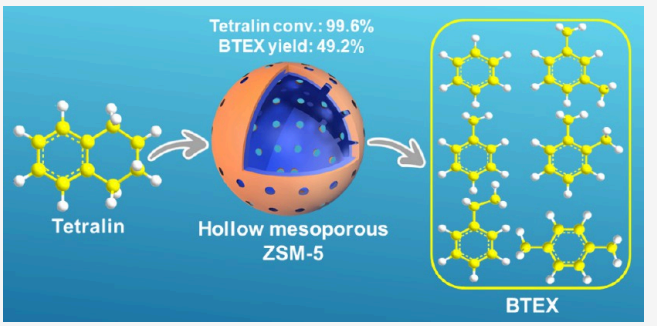

1. INTRODUCTION

Heavy aromatics, which generally refer to monocyclic and bicyclic alkyl aromatic hydrocarbons of C_9 or above, mainly come from catalytic reforming, steam cracking, and catalytic cracking units. Due to the similar boiling points of the components, it is particularly difficult to isolate a single high value-added product from heavy aromatics, and most of them are consumed as low-quality fuels.[1] This way of utilization not only wastes the aromatic resources but also causes environmental concerns.[2] Light aromatics such as benzene, toluene, ethylbenzene, and xylene (BTEX) are the most important chemical feedstocks, as they are building blocks for producing commodity chemicals in the petrochemical industry. Therefore, upgrading heavy aromatics into high-value BTEX has gained considerable attention.

Conversion of heavy aromatics to BTEX involves hydrogenation of aromatic rings as well as isomerization, ring opening, and dealkylation reactions.[3−5] The zeolite catalysts including ZSM-5, Y, β, and MOR have been used in this conversion process.[6−10] Among them, ZSM-5 zeolite has become one of the most widely used catalysts and was first synthesized by Mobil Corporation in 1972. Due to its unique pore structure, good hydrothermal stability, and adjustable acid properties, ZSM-5 has demonstrated excellent catalytic activity in acid catalytic reactions such as alkylation, isomerization, and arylation in the petrochemical field.[11−16] Conventional ZSM-5 zeolites possess a microporous structure with long and small microporous channels, which limit the diffusion efficiency of macromolecular reactants and products within the zeolites, leading to poor catalytic performance.[17] In addition, large molecules such as heavy aromatics may polymerize in the microporous channels and eventually turn into coke to cover the active sites and block the channels, resulting in rapid deactivation of catalyst.[18] Therefore, modulation of the pore structure of ZSM-5 is an effective strategy to improve the catalytic performance of reactions related to large molecules.[19,20] Creation of meso- and macropores in microporous

Received: November 13, 2024
Revised: February 4, 2025
Accepted: February 5, 2025
Published: February 13, 2025

https://doi.org/10.1021/acs.iecr.4c04323
Ind. Eng. Chem. Res. 2025, 64, 4330−4341

zeolites can solve the diffusion limitations of large molecules in the zeolites, thus enhancing the catalytic activity and extending the lifespan of zeolite catalysts.[21,22]

Treating zeolites in an alkaline environment is a general approach to create mesopores within the zeolites by removing framework silicon.[23] Dai et al. prepared ZSM-5 with hollow or mesoporous structure by controlling the concentration of TPAOH and the alkali treatment duration.[24] Ma et al. prepared hollow mesoporous ZSM-5 with large mesopore size (~23 nm) by treating S-1 zeolite using $NaAlO_2$ and TPAOH.[25] Fu et al. introduced abundant mesopores (4−12 nm) in the shell of hollow nano-ZSM-5 using a mixed solution of NaOH and TPAOH.[26] Xu et al. synthesized hollow mesoporous ZSM-5 with mesopore size ranging from 7.9 to 20.5 nm using a mixed alkali solution of NaOH and TPAOH.[20] Currently, the mesopores in hollow mesoporous ZSM-5 synthesized through alkali treatment are large and uneven, and the fine-tuning of mesopore sizes remains a challenge. Since uniform and controllable pore sizes are crucial for catalytic efficiency and selectivity, it is necessary to develop a method for preparing hollow mesoporous ZSM-5 with uniform and adjustable mesopores.

In this study, we synthesized hollow mesoporous ZSM-5 zeolites with tunable mesopore sizes ranging from 2 to 12 nm by a facile one-step mixed alkali treatment using TPAOH and Na_2CO_3. The mesopore diameter could be easily adjusted by changing the concentration of Na_2CO_3. Additionally, the effects of alkali treatment time, Si/Al ratio of parent ZSM-5, and zeolite/solution ratio on the formation of mesopores were investigated. The catalytic performance of the hollow mesoporous ZSM-5 catalysts was evaluated by using the conversion of tetralin to BTEX as a model reaction. Compared to parent ZSM-5 and hollow ZSM-5, the hollow mesoporous ZSM-5 exhibited enhanced tetralin conversion and BTEX yield, reaching 99.6% and 49.2%, respectively.

2. EXPERIMENTAL SECTION

2.1. Catalyst Synthesis. *Synthesis of Parent ZSM-5 (P-Z5).* Parent ZSM-5 was synthesized by a hydrothermal method. In a typical synthesis, a mixture of 200.86 g of tetrapropylammonium hydroxide solution (TPAOH, 25%), 190.50 g of tetraethyl orthosilicate (TEOS, >98%), and 260.85 g of deionized water was stirred and hydrolyzed for 3 h to form solution A. Solution B was prepared by dissolving 4.67 g of aluminum isopropoxide (AIP, AR) in 197.55 g of deionized water. After complete hydrolysis of solution A, solution B was slowly added dropwise to solution A. The resulting mixture was transferred into an autoclave and kept at 170 °C in an oven for 72 h. The product was then centrifuged and washed to neutrality. After drying at 80 °C, it was calcined in a muffle furnace at 540 °C for 4 h to obtain P-Z5 with theoretical Si/Al ratio of 40. Parent ZSM-5 with theoretical Si/Al ratios of 60, 80, and 100 were also synthesized according to the same procedure except that the amounts of AIP are 7.01, 9.34, and 11.68 g, respectively.

Synthesis of Hollow ZSM-5 (HM-∞) and Hollow Mesoporous ZSM-5 (HM-x). Hollow mesoporous ZSM-5 was prepared by treating P-Z5 with a mixed alkali solution of TPAOH (25%) and sodium carbonate (Na_2CO_3, AR). Typically, 2 g of P-Z5 was added into 60 mL of a mixed alkali solution with a specific molar ratio of TPAOH to Na_2CO_3. The mixture was then put into a 100 mL autoclave, which was subsequently treated in a rotating oven at 170 °C with a rotation speed of 60 rpm for 72 h. After cooling down to room temperature, the solid product in the autoclave was centrifuged, washed with deionized water until neutrality, and dried overnight at 80 °C. The dried product was then calcined at 540 °C for 6 h. Subsequently, the resulting white powder was subjected to ammonium exchange by placing it in a 1.0 M NH_4NO_3 solution with a zeolite/solution ratio of 1:10 at 80 °C for three cycles, with each cycle lasting 2 h. After the exchange, the catalyst was centrifuged, washed to neutrality, and dried at 80 °C. Finally, the white powder was calcined in a muffle furnace at 540 °C for 4 h. The final product, hollow mesoporous ZSM-5, was denoted as HM-x, where x represents the molar ratio of TPA^+/Na^+ (x = 54, 27, 18, 9, 1.35, 0.675, 0.54, and 0.45). The concentration of TPAOH was kept at 0.27 M, and that of Na_2CO_3 was varied to adjust the TPA^+/Na^+ ratio from 54 to 0.45. For the investigation of the effect of zeolite/solution ratio, the volumes of the added mixed alkali solution were 20 and 30 mL when the zeolite/solution ratios were 1:10 and 1:15, respectively.

Hollow ZSM-5 (HM-∞) was synthesized according to the same procedure as the synthesis of hollow mesoporous ZSM-5 except that Na_2CO_3 was not added.

2.2. Characterizations. X-ray diffraction (XRD) patterns were collected on a Rigaku Smartlab 9 kW diffractometer equipped with Cu Kα radiation (λ = 1.5418 Å, 40 kV, 100 mA) in the range of 2θ = 5−80° at a scanning rate of 5° min^{-1}. Scanning electron microscopy (SEM) images were obtained using a Hitachi SU8200 instrument with an accelerating voltage of 5 kV to observe the morphology and crystal size of the samples. Transmission electron microscopy (TEM) images were recorded on a Thermo TF30 electron microscope with an accelerating voltage of 300 kV. N_2 adsorption−desorption isotherms were performed on an Autosorb-iQ physisorption analyzer (Quantachrome Corporation, USA) at −196 °C to determine the specific surface area and pore structure information on the catalysts. Prior to testing, the samples were degassed at 300 °C for 6 h. The specific surface area was calculated using the BET (Brunauer−Emmett−Teller) method; the total pore volume was determined from the nitrogen amount adsorbed at a relative pressure P/P_0 of 0.99, and the micropore volume was calculated using the t-plot method. Temperature-programmed desorption of ammonia (NH_3-TPD) data were recorded from room temperature to 700 °C with a ramping rate of 10 °C min^{-1} on a ChemBET Pulsar TPR/TPD automatic chemical adsorption instrument (Quantachrome) with a TCD detector to detect the NH_3 desorption signal. The actual Si/Al ratios were analyzed using inductively coupled plasma-optical emission spectroscopy (ICP-OES, PerkinElmer Avio 500). Thermogravimetric analysis (TGA) was performed on a thermal analyzer (SDT Q600, TA Instruments) from room temperature to 1000 °C with a ramping rate of 10 °C min^{-1} in air. ^{27}Al MAS NMR experiments were conducted on a Bruker Avance III spectrometer at 14.1 T (1H Larmor frequency at 600.13 MHz) using a 3.2 mm HXY probe with an MAS rate of 16 kHz. ^{27}Al single-pulse MAS NMR spectra were recorded with a pulse width of 0.8 μs corresponding to a $\pi/12$ flip-angle, a recycle delay of 1, and 2048 scans. ^{27}Al chemical shifts are referenced to a 1 M $Al(NO_3)_3$ solution at 0 ppm. The Brønsted and Lewis acid sites of the samples were analyzed with pyridine infrared (Py-IR) spectra on a Nicolet iS20 spectrometer. The adsorption of pyridine was carried out at room temperature, and then the physisorbed pyridine

https://doi.org/10.1021/acs.iecr.4c04323
Ind. Eng. Chem. Res. 2025, 64, 4330−4341

molecules and that in the gas were removed under vacuum at 200 °C for 30 min. When the temperature was reduced to room temperature, the spectra were recorded.

The diffusion property of the catalysts was characterized using an intelligent gravimetric analyzer (IGA100, Hiden Isochema Ltd., Warrington, UK). The sample (40−50 mg) was subjected to an analysis using ortho-xylene molecule as adsorbate at a temperature of 25 °C and a pressure of 5 mbar. The diffusion time constants were obtained by fitting the uptake profiles according to eq 1:[27,28]

$$\frac{q(t)}{q(m)} = \frac{6}{\sqrt{\pi}}\sqrt{\frac{D}{r^2}}\sqrt{t} \quad (1)$$

2.3. Catalytic Performance Evaluation. The catalytic performance of the catalysts was evaluated using hydrocracking of tetralin to BTEX as a model reaction. The reaction was carried out in a fixed-bed reactor at 400 °C and 2 MPa. Prior to reaction, the catalyst was pelletized (20−40 mesh), mixed with an appropriate amount of quartz sand (20−40 mesh), and loaded into the reaction tube. The reactor was heated to 400 °C under a hydrogen (H_2) atmosphere. Tetralin ($C_{10}H_{12}$, >98.4%) was injected into a preheated furnace (400 °C) through a piston pump. After vaporization, it was mixed with H_2 at the beginning of the insulation section (400 °C), and then the mixture entered the reactor to start reaction under the effect of a catalyst. After the reaction, the products were cooled in a condenser at 5 °C and the liquid products were separated. The collected liquid products were analyzed using an Agilent 6890N gas chromatograph.

The conversion of tetralin (X_{TL}) and the yield of BTEX (Y_{BTEX}) were calculated using the following formulas:

$$X_{TL} = \frac{m_{TL,in} - x \times m_{out}}{m_{TL,in}} \times 100\% \quad (2)$$

$$Y_{BTEX} = S_{BTEX} \times Y_L \quad (3)$$

$$Y_L = \frac{m_{out}}{m_{TL,in}} \times 100\% \quad (4)$$

where $m_{TL,in}$ represents the mass of tetralin that is pumped into the system, m_{out} represents the mass of collected liquid phase product, x represents the percentage of tetralin in the liquid phase product, and Y_L and S_{BTEX} represent liquid yield and BTEX selectivity, respectively.

3. RESULTS AND DISCUSSION

3.1. Regulation of Mesopore Size of Hollow Mesoporous ZSM-5. Hollow mesoporous ZSM-5 (HM-x) was obtained through a one-step alkali treatment of P-Z5 (theoretical Si/Al = 40 and actual Si/Al = 61). Figure 1 displays the XRD patterns of P-Z5, HM-∞, as well as HM-x samples treated with mixed alkali solutions of varying molar ratios of TPAOH to Na_2CO_3. All samples exhibit five characteristic peaks at 7.69°, 8.83°, 23.18°, 23.99°, and 24.45°, indicating that they possess the typical MFI topological structure of ZSM-5 zeolite,[29] and the mixed alkali treatment does not destroy the MFI structure. However, the intensity of the diffraction peaks of the alkali treated samples is reduced to varying degrees compared to P-Z5, indicating a decrease in crystallinity due to the extraction of silicon species from the zeolite framework after alkali treatment. To characterize the change in crystallinity, the relative crystallinity of P-Z5 and

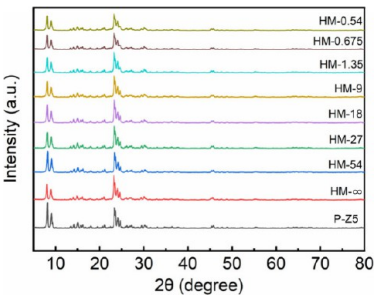

Figure 1. XRD patterns of P-Z5, HM-∞, and HM-x.

HM-x was calculated. The crystallinity of a sample was represented by the sum of the areas of the above five characteristic peaks. Taking the crystallinity of P-Z5 as 100%, the relative crystallinity of other samples was obtained (Table S1). After mixed alkali treatment, the crystallinity of HM-x gradually decreases with decreasing x value, i.e., the increase of Na_2CO_3 concentration. When the TPA^+/Na^+ ratio decreases to 0.54, the crystallinity of HM-0.54 drops to 76%.

The SEM images of P-Z5, HM-∞, as well as HM-x are displayed in Figure 2. It can be seen that the morphology of ZSM-5 is retained after alkali treatment; however, the surface of the HM-x zeolites becomes rough, in contrast to P-Z5 with smooth surface. Moreover, the surface roughness increases with increasing inorganic alkali concentration, which can be attributed to the formation of mesopores on the surface of ZSM-5 due to alkali etching. In addition, excessive concentration of inorganic alkali leads to the fracture of hollow structure (Figure 2g-i). The TEM images of the samples are shown in Figures S1 and 3. It can be seen that P-Z5 is solid, while HM-∞ exhibits a hollow structure without mesopores (Figures S1). By contrast, the mesopores in the shell of the hollow zeolites can be clearly observed for the HM-x samples (Figure 3). As the concentration of Na_2CO_3 increases, the mesopore diameter gradually increases from 2 to 12 nm, as can be seen from the corresponding mesopore size distribution plots (Figure 3a3-h3). However, excess Na_2CO_3 addition leads to a fragmentation phenomenon (Figure 3f-h), consistent with the SEM observations. This is because excessively high concentration of Na^+ cations results in uncontrollable desilication, and thus the zeolite structure is destroyed.[30]

The above hollow mesoporous ZSM-5 was obtained by treating P-Z5 at 170 °C for 72 h with a mixed alkali solution of TPAOH and Na_2CO_3. The effect of alkali treatment time on the formation of mesoporous structure was investigated, and the samples obtained by treating P-Z5 in mixed alkali solution for different durations were denoted as HM-x-yh, where x and y represent the ratio of TPA^+/Na^+ and the alkali treatment duration, respectively. XRD patterns (Figure S2) confirm that all samples possess a typical MFI topological structure. The SEM images (Figure S3) reveal that the treatment time does not affect the morphology of ZSM-5. When the treatment time is shorter (6−24 h), some debris can be observed (Figure S3c,e), which may be due to the etching of amorphous silica from the interior of ZSM-5. As the alkali treatment time is extended to 72 h (Figure 2e,f), this phenomenon disappears, and the zeolite structure is intact. This may be due to the secondary crystallization induced by TPAOH; that is, the etched amorphous silica recrystallizes on the outer surface of ZSM-5.[31] From the TEM images (Figure 4), we can see that

https://doi.org/10.1021/acs.iecr.4c04323
Ind. Eng. Chem. Res. 2025, 64, 4330−4341

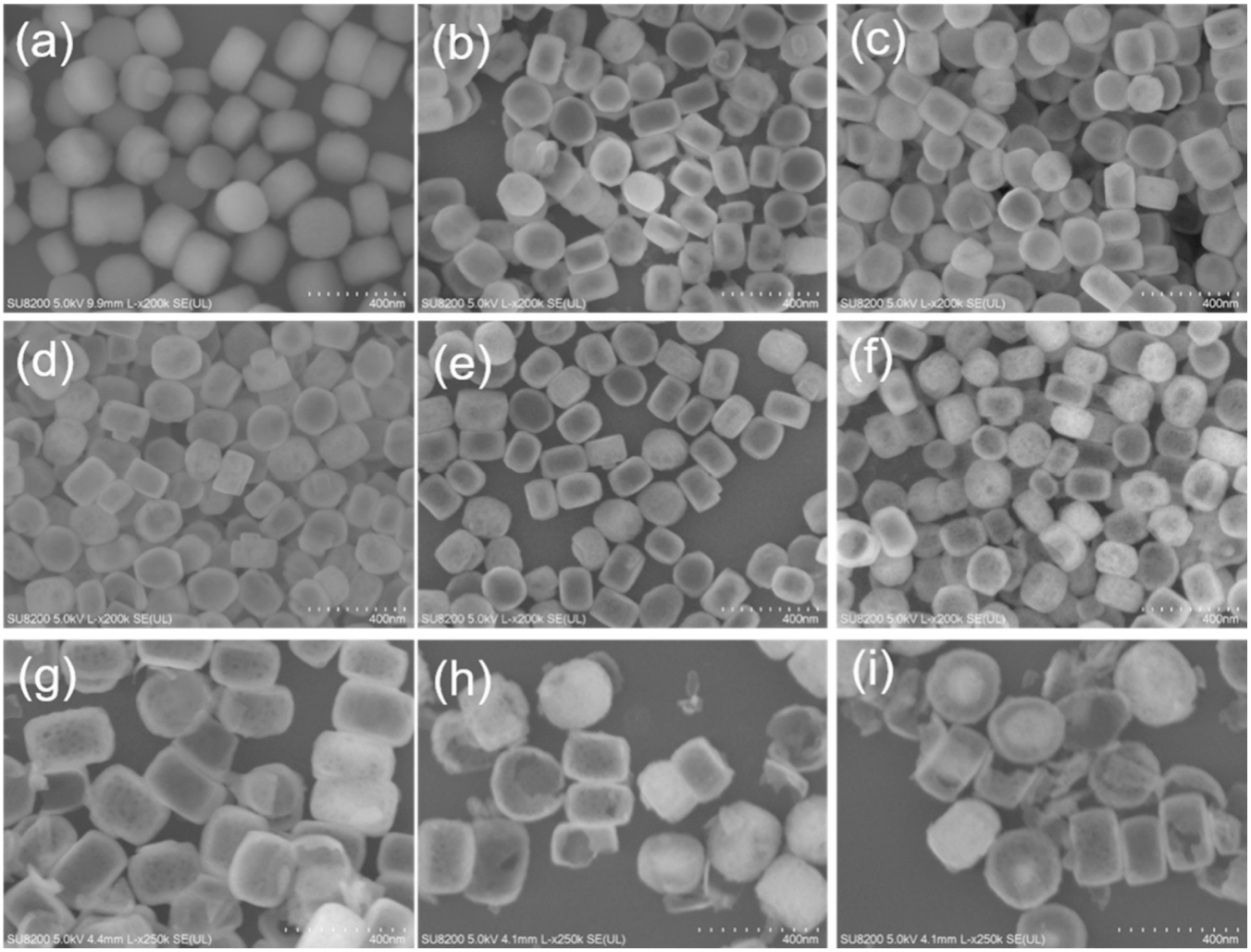

Figure 2. SEM images of P-Z5 (Si/Al = 61), HM-∞, and HM-x samples: (a) P-Z5, (b) HM-∞, (c) HM-54, (d) HM-18, (e) HM-9, (f) HM-1.35, (g) HM-0.675, (h) HM-0.54, and (i) HM-0.45.

when the treatment time is short, some zeolite grains do not form a hollow structure. As the treatment time is prolonged, almost all of the zeolite grains become hollow. This is because the parent ZSM-5 is first etched to form mesopores, which are interconnected to form a larger cavity. When the concentration of Na_2CO_3 is low, the mesopore size changes little with an extended treatment time. The pore size distribution plots show that the mesopores of HM-9−6h, HM-9−12h, and HM-9−24h are distributed around 6−7 nm (Figure 4a3-c3), while those of HM-9−72h are sized between 7−8 nm (Figure 3d3). In contrast, when the alkali concentration is high, significant mesopores can be observed in a short time and the size of mesopores increases with the duration of alkali treatment. The mesopores of HM-1.35−6h, HM-1.35−12h, and HM-1.35−24h are concentrated around 6−8 nm (Figure 4d3-f3), whereas those of HM-1.35−72h grow to approximately 10−12 nm (Figure 3e3).

The influence of the Si/Al ratio of parent ZSM-5 on the mesopore size under identical alkali treatment conditions (TPA^+/Na^+ = 1.35) was also investigated. The actual Si/Al ratios are 61, 76, 105, and 128 for parent ZSM-5 prepared with theoretical Si/Al ratios of 40, 60, 80, and 100, respectively. As the Si/Al ratio of parent ZSM-5 increases, the shell thickness of the hollow cavity decreases, from approximately 25 nm for Si/Al = 61 (Figure 3e1,e2) to around 18 nm for Si/Al = 128 (Figure 5c1,c2). This is because the increased silicon content in the zeolite with a higher Si/Al ratio leads to a greater degree of etching by the mixed alkali solution and consequently a reduction in shell thickness. In addition to the change of shell thickness, the size and distribution of the mesopores also change to some extent with the increase of the Si/Al ratio. For the parent ZSM-5 with Si/Al ratio of 61, the mesopore size is around 10−11 nm (Figure 3e3), and it increases to about 14−16 nm with a wider distribution range of 6−38 nm when the Si/Al ratio is 128 (Figure 5c3). This can be ascribed to the increased silicon content with a higher Si/Al ratio, which results in a serious etching effect at the same alkali concentration, probably connecting two or more smaller mesopores to form a larger one. SEM images also reveal that under the same alkali treatment condition, the samples obtained by treating parent ZSM-5 with high Si/Al ratios (105 and 128) exhibit an obvious fragmentation phenomenon (Figure S4c,d). This is because the increased Si content makes the etching easier, leading to the break of the hollow structure.

We further investigated the influence of the zeolite/solution ratio on the formation of a hollow mesoporous structure in ZSM-5 zeolite. During the investigation of the effect of the zeolite/solution ratio, the concentration of the mixed alkali was

https://doi.org/10.1021/acs.iecr.4c04323
Ind. Eng. Chem. Res. 2025, 64, 4330−4341

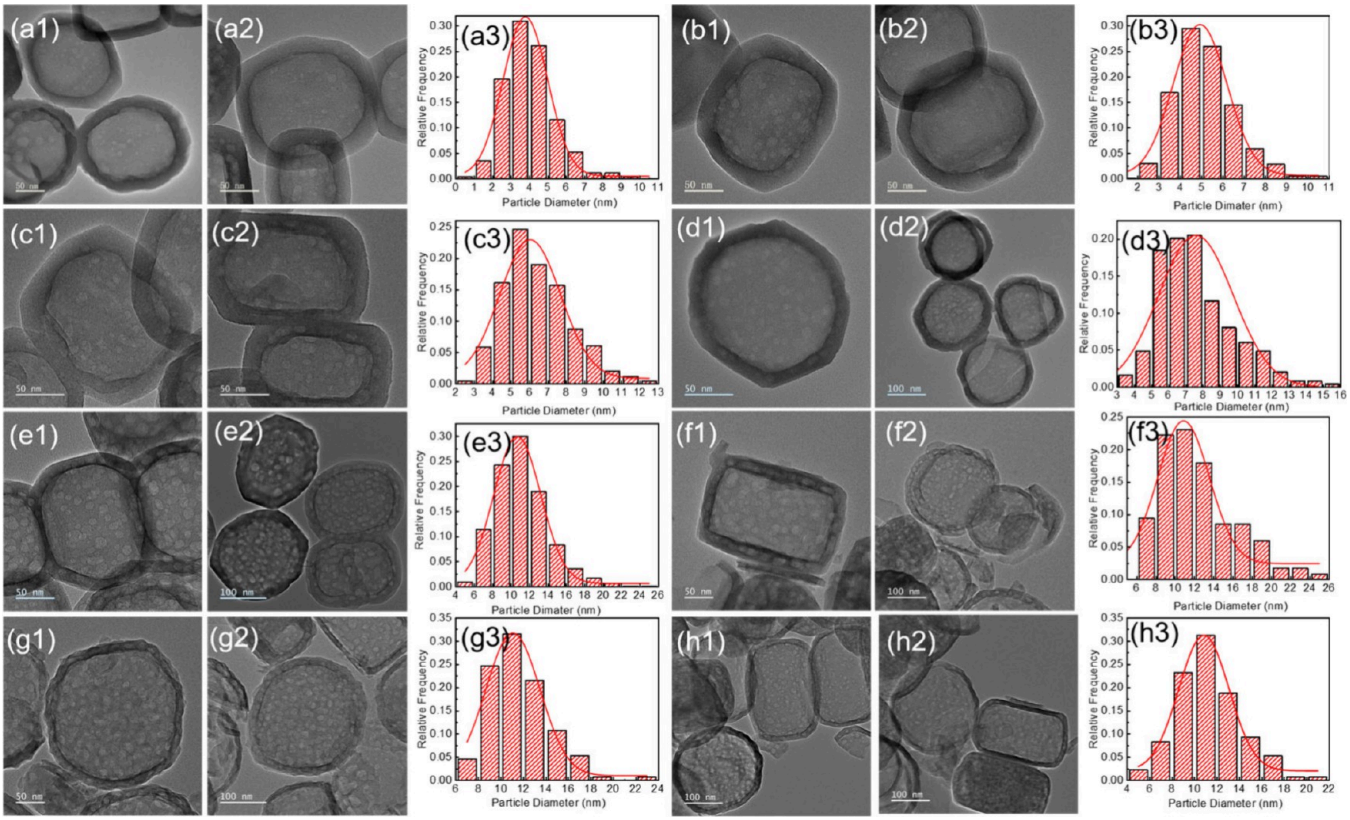

Figure 3. TEM images of HM-x and the corresponding pore size distributions: (a1−a3) HM-54, (b1−b3) HM-27, (c1−c3) HM-18, (d1−d3) HM-9, (e1−e3) HM-1.35, (f1−f3) HM-0.675, (g1−g3) HM-0.54, and (h1−h3) HM-0.45 (Pore size distributions are obtained by measuring more than 200 pores of the TEM images).

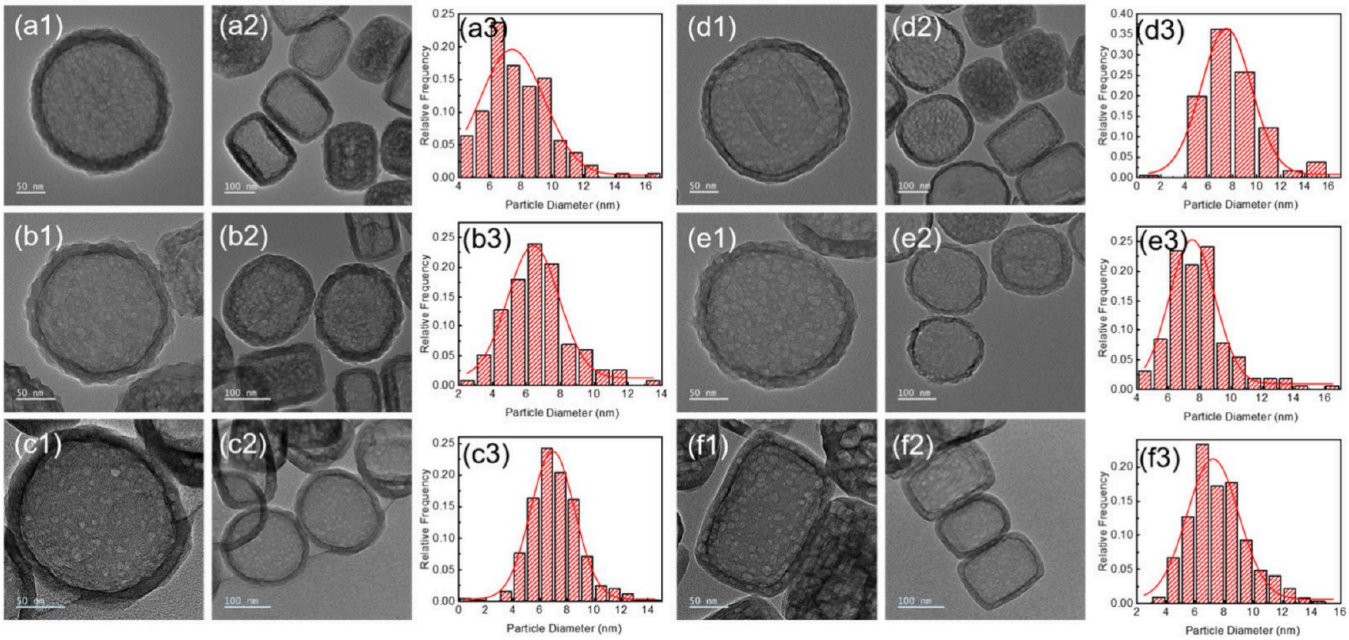

Figure 4. TEM images of HM-9 and HM-1.35 treated at different durations and the corresponding pore size distributions: (a1-a3) HM-9−6h, (b1-b3) HM-9−12h, (c1-c3) HM-9−24h, (d1-d3) HM-1.35−6h, (e1-e3) HM-1.35−12h, and (f1-f3) HM-1.35−24h (Pore size distributions are obtained by measuring more than 200 pores of the TEM images).

kept constant, while the volume of the alkali was changed. Therefore, increasing the zeolite/solution ratio led to a decrease of the amount of TPA^+ and OH^- in the solution. From the SEM images in Figure S5, it can be observed that some fragments appear when the zeolite/solution ratios are 1:10 and 1:15. This is because the degree of secondary crystallization of amorphous silica was not complete due to the insufficient TPA^+ in the solution, resulting in the formation of

https://doi.org/10.1021/acs.iecr.4c04323
Ind. Eng. Chem. Res. 2025, 64, 4330−4341

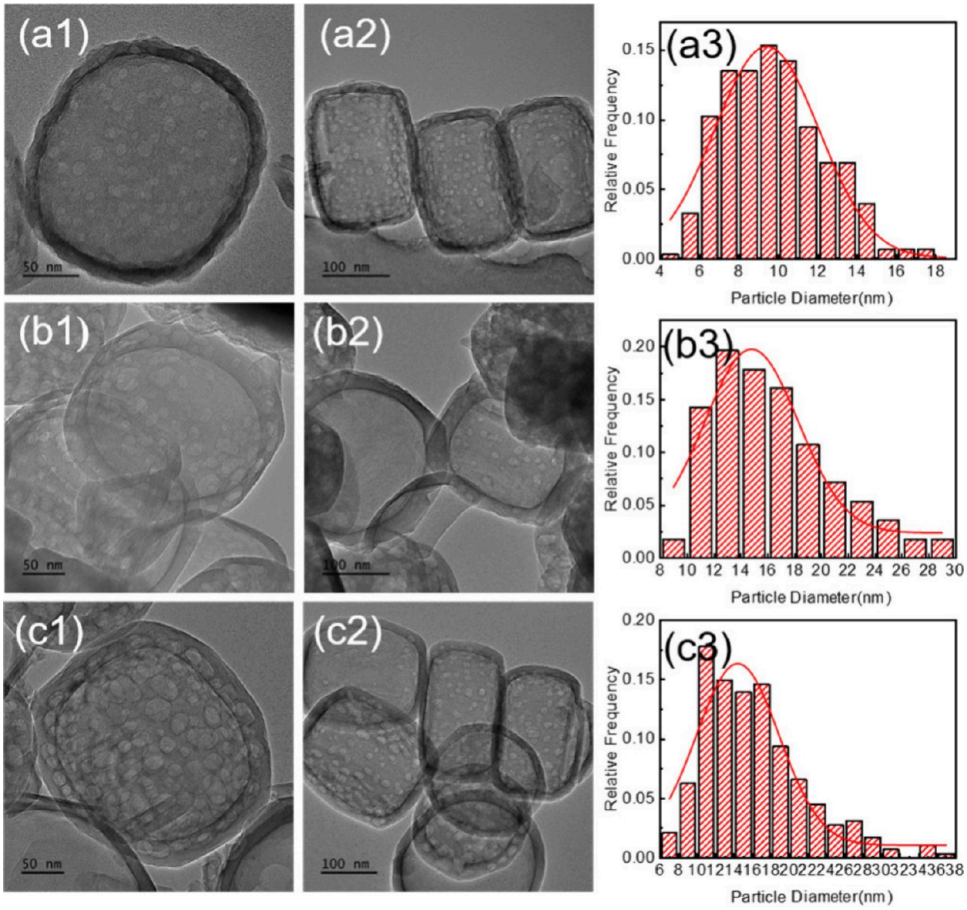

Figure 5. TEM images of the samples obtained by treating parent ZSM-5 with different Si/Al ratios under the same alkali treatment condition of TPA^+/Na^+ = 1.35: (a1−a3) Si/Al = 76, (b1−b3) Si/Al = 105, and (c1−c3) Si/Al = 128 (Pore size distributions are obtained by measuring more than 200 pores of the TEM images).

some irregular fragments on the outer shell. Moreover, no discernible mesopores can be observed from the TEM images (Figure S6). This is due to the reduction in the amount of OH^-, leading to insufficient etching to produce mesopores. By contrast, when the zeolite/solution ratio is decreased to 1:30, the presence of mesopores can be clearly found (Figure 3d1,d2). These findings indicate that the zeolite/solution ratio also plays a critical role in the generation of mesopores within the zeolite framework.

3.2. Characterizations of Hollow Mesoporous ZSM-5.

Figure 6a shows the N_2 adsorption−desorption isotherms of the P-Z5, HM-∞, and HM-x samples. The isotherms of P-Z5 belong to type I, characteristic of microporous materials.[29,32] Hollow ZSM-5 (HM-∞) and hollow mesoporous ZSM-5 (HM-x) exhibit type IV isotherms and an H2-type hysteresis loop, with a sharp decrease in the desorption branch at around P/P_0 = 0.5. The nitrogen adsorption behavior of hollow zeolites in the region of low relative pressure is similar to that of the parent zeolite, whereas in the region of high relative pressure, the nitrogen adsorption capacity of the hollow zeolites is greater than that of the parent one, as nitrogen also fills in the hollow cavities in addition to the interparticle mesopores. The corresponding pore size distribution plots of HM-x (Figure 6b) show an obvious prominence in the range of 3−15 nm, indicating the presence of mesopores in the samples.

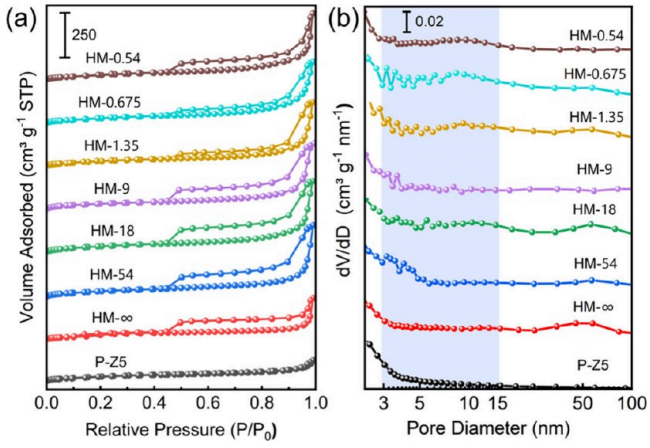

Figure 6. (a) N_2 adsorption−desorption isotherms and (b) the corresponding pore size distribution plots of P-Z5, HM-∞, and HM-x.

The BET specific surface area and pore structure information on the samples are listed in Table S2. Compared to P-Z5, the specific surface areas of the hollow mesoporous samples are reduced. With an increase in the concentration of Na_2CO_3, the specific surface area generally exhibits a decreasing trend, dropping from the initial surface area of 463 $m^2\ g^{-1}$ for P-Z5 to 368 $m^2\ g^{-1}$ for HM-0.54. The micropore specific surface area also shows a significant

https://doi.org/10.1021/acs.iecr.4c04323
Ind. Eng. Chem. Res. 2025, 64, 4330−4341

decrease from 407 m^2 g^{-1} for P-Z5 to 263 m^2 g^{-1} for HM-0.54. By contrast, the total pore volume increases from 0.23 cm^3 g^{-1} for P-Z5 to 0.40 cm^3 g^{-1} for HM-∞, and then to about 0.60 cm^3 g^{-1} for HM-x, which changes little when treated in alkali with different concentrations. However, the micropore volume gradually decreases from P-Z5 to HM-∞ and then to HM-x. As the alkali concentration increases, more micropores are interconnected to form larger meso- or macropores, leading to a reduction in micropore volume. At the same time, the mesopore and macropore volumes generally show an increasing trend, from 0.05 cm^3 g^{-1} for P-Z5 to 0.51 cm^3 g^{-1} for HM-0.54, confirming the presence of mesopores and macropores in the HM-x samples. The increase in mesopore volume with alkali concentration is also consistent with the mesopore size from the TEM observations.

The acidity of P-Z5 and alkali-treated samples was investigated by NH_3-TPD. The NH_3-TPD profiles and the derived acidity data are presented in Figure 7 and Table 1,

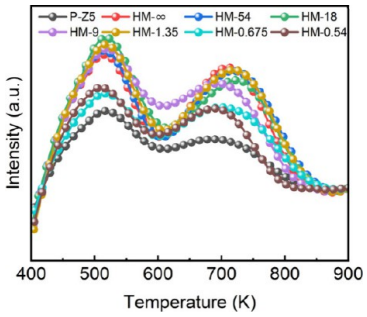

Figure 7. NH_3-TPD profiles of P-Z5, HM-∞, and HM-x.

Table 1. Si/Al ratios determined by ICP and acid amounts of P-Z5, HM-∞, and HM-x

Sample	Si/Al ratio	Acid amount (μmol g^{-1})			
		Total	$C_{Weak}(T_1, K)$	$C_{Medium\ strong}(T_2, K)$	$C_{Strong}(T_3, K)$
P-Z5	61	114	59(517)	29(643)	28(729)
HM-∞	45	220	99(515)	48(655)	73(731)
HM-54	45	228	104(517)	55(663)	72(745)
HM-18	40	231	114(517)	46(649)	74(739)
HM-9	45	222	104(517)	56(633)	66(722)
HM-1.35	47	232	108(518)	52(656)	75(740)
HM-0.675	48	168	74(517)	48(654)	48(743)
HM-0.54	48	155	78(516)	37(645)	40(732)
P-Z5*[a]	38	240	120(517)	56(648)	64(742)

[a]P-Z5* represents solid ZSM-5 with similar acid amount to HM-18.

respectively. Two distinct NH_3 desorption peaks at 520 and 730 K correspond to the weak and strong acid centers of ZSM-5 zeolite, and the area of the desorption peaks reflects the amount of acid.[33] The acid amount of P-Z5 is 114 μmol g^{-1}, and it increases to 220 μmol g^{-1} for HM-∞. The acid amount of HM-x obtained through the mixed alkali treatment does not differ significantly from that of HM-∞. However, when the concentration of Na_2CO_3 increases to a certain level, the acid amount decreases; for instance, the acid amount of HM-0.675 is 168 μmol g^{-1}. This is because only Si species in the zeolite are dissolved in the mixed alkali solution with low concentration Na_2CO_3, while Al acid sites are exposed on the zeolite surface. However, in the alkali solution with a high concentration of Na_2CO_3, both framework Si and Al are removed during the alkali treatment process, leading to a reduction in the acidity of the samples.

Pyridine infrared (Py-IR) spectra were employed to characterize the Brønsted acid site (BAS) and Lewis acid site (LAS) of the samples. As depicted in Figure 8, the absorption

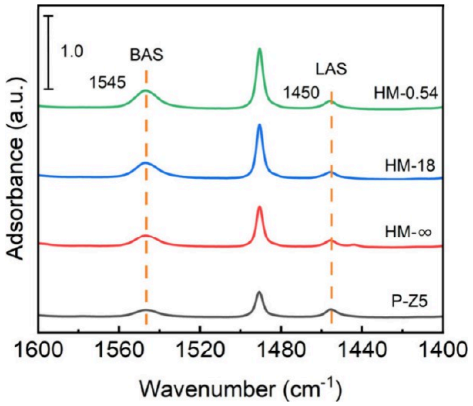

Figure 8. Py-IR spectra of P-Z5, HM-∞, HM-18, and HM-0.54 recorded at 200 °C.

peaks at 1545 and 1450 cm^{-1} correspond to the characteristic absorptions of BAS and LAS, respectively.[34,35] Compared to P-Z5, the samples subjected to alkali treatment including HM-∞, HM-18, and HM-0.54 exhibit a significant increase in the amount of BAS (Table 2). As the alkali concentration

Table 2. Amount of Brønsted and Lewis acid sites for P-Z5, HM-∞, HM-18, and HM-0.54 obtained from Py-IR spectra

Sample	Acid amount[a] (μmol g^{-1})		
	Brønsted	Lewis	B/L
P-Z5	65.4	33.1	2.0
HM-∞	98.9	29.1	3.4
HM-18	140.0	26.1	5.4
HM-0.54	170.7	33.2	5.1

[a]$C_{(pyridine\ on\ B\ sites)}$ = 1.88 IA(B)R^2/W and $C_{(pyridine\ on\ L\ sites)}$ = 1.42 IA(L)R^2/W (R = 0.7 cm, W = 20 mg).

increases, the BAS shows a gradual increase, while the LAS remains relatively stable, and the ratio of BAS to LAS (B/L) first increases and then slightly decreases. The difference of chemical state of Al before and after alkali etching treatment was investigated using ^{27}Al MAS NMR spectroscopy. Figure S7 presents the ^{27}Al MAS NMR spectra of P-Z5 and HM-18. The peak at 0 ppm corresponds to hexa-coordinated nonframework aluminum, while the peak at 55 ppm corresponds to tetra-coordinated framework aluminum.[36,37] It can be seen that the amount of nonframework aluminum in HM-18 decreases compared to that of P-Z5, because nonframework aluminum are dissolved and some of them are converted to framework aluminum during the process of mixed alkali treatment,[24] consistent with the increased BAS from Py-IR spectra.

3.3. Formation Mechanism of Hollow Mesoporous ZSM-5. Alkali treatment is a widely used strategy to create hollow or mesoporous structure in zeolites, during which alkali etches silicon from the zeolite framework. Alkali preferentially etches the interior of ZSM-5 zeolite because ZSM-5 synthesized using TPAOH as a template agent has an

https://doi.org/10.1021/acs.iecr.4c04323
Ind. Eng. Chem. Res. 2025, 64, 4330−4341

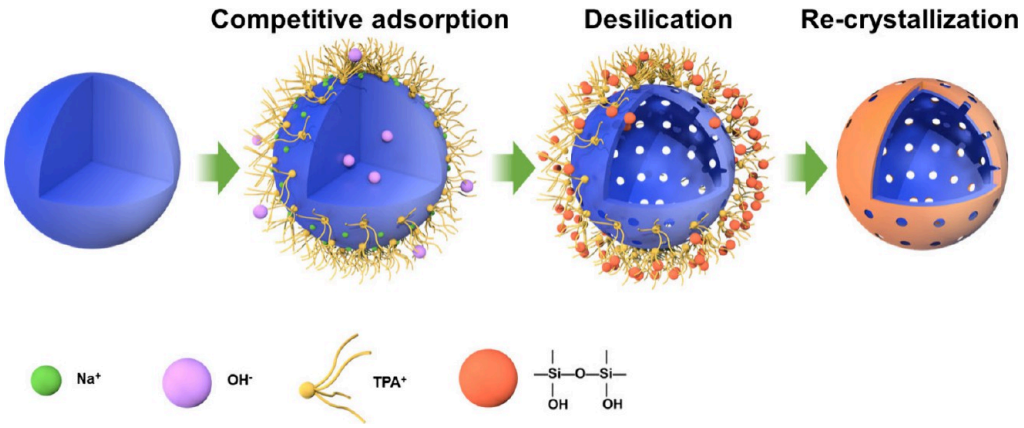

Figure 9. Scheme of the formation mechanism of hollow mesoporous ZSM-5.

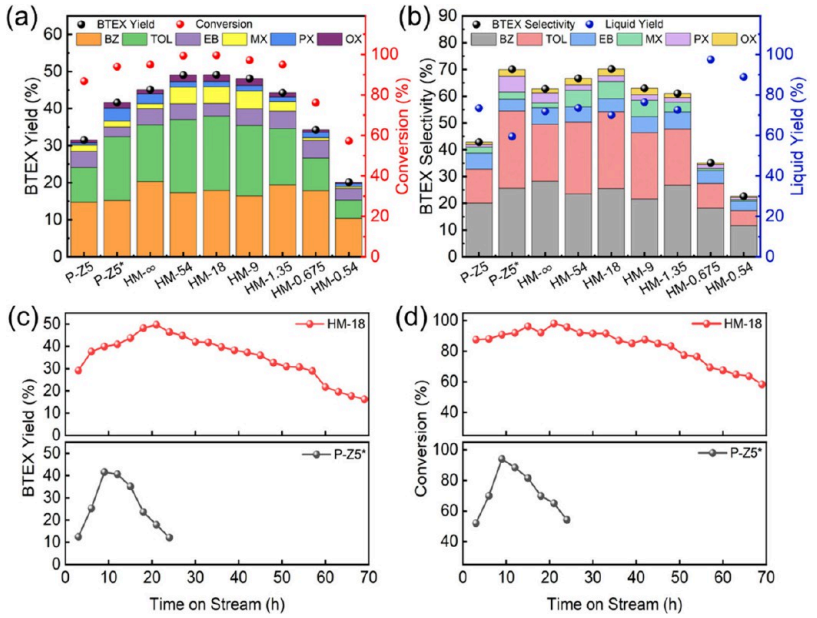

Figure 10. (a) BTEX yield and tetralin conversion and (b) BTEX selectivity and liquid yield of P-Z5, P-Z5*, HM-∞, and HM-x, (c) BTEX yield and (d) tetralin conversion of P-Z5* and HM-18 during long-term operation: (P-Z5* represents solid ZSM-5 with similar acid amount to HM-18; BZ, TOL, EB, MX, PX, and OX represent benzene, toluene, ethylbenzene, meta-xylene, para-xylene, and ortho-xylene, respectively). Reaction conditions: 0.46 g of catalyst, 400 °C, 2 MPa, WHSV = 1 h^{-1}, H_2/tetralin = 800 (volume ratio).

aluminum-rich exterior and a silicon-rich interior.[38−40] The EDS line scan profile of aluminum element (Figure S8) exhibits a shape of high on both sides and low in the middle, which proves that aluminum is more distributed in the outer layer of the zeolites. A high framework aluminum concentration on the surface prevents silicon extraction, while a high silicon concentration in the interior makes the extraction of silicon easier, leading to the formation of a large cavity. In the presence of TPA^+, the negatively charged framework aluminum on the outer surface of ZSM-5 attracts TPA^+ cations with positive charge through electrostatic interaction. Since the size of TPA^+ (0.85 nm) exceeds the pore diameter of ZSM-5 (0.56 nm),[41] TPA^+ cations adsorbed onto the outer surface of the zeolite also protect the silicon from being etched by OH^-.[42] Therefore, when treated solely with TPAOH, only hollow cavities in the ZSM-5 zeolite are formed.

Figure 9 illustrates the formation mechanism of hollow mesoporous ZSM-5 in the presence of TPAOH and Na_2CO_3. When the inorganic base Na_2CO_3 is introduced, both TPA^+ and Na^+ cations are competitively adsorbed on the external surface of ZSM-5. Unlike TPA^+, the region adsorbed with Na^+ lacks the protective effect on Si; therefore, Si species are etched by alkali and mesopores are formed. As the concentration of inorganic base increases, the amount of adsorbed Na^+ also increases, leading to an increased number of mesopores. The interconnection of adjacent small mesopores will form larger mesopores. The hollow mesoporous ZSM-5 is formed under the combined effects of the protective effect of TPA^+ and the competitive adsorption of Na^+.

3.4. Catalytic Performance of HM-x for Hydrocracking of Tetralin to BTEX. The catalytic performance of P-Z5, HM-∞, and HM-x were evaluated using hydrocracking of tetralin to BTEX as a model reaction, and the results are shown in Figure 10 and Table S3. The performance data are average values between the ninth and 19th hour after the reaction begins since the reaction at this stage is relatively stable. It should be noted that metal was not introduced during the preparation of the catalysts; therefore, there was no hydro-

https://doi.org/10.1021/acs.iecr.4c04323
Ind. Eng. Chem. Res. 2025, 64, 4330−4341

genation active component, and only the acid sites played a role in the reaction. As shown in Figure 10a, the conversion of tetralin and the BTEX yield of P-Z5 are 86.8% and 31.6%, respectively. By contrast, HM-∞ and HM-x exhibit significantly improved catalytic activity. Especially, the tetralin conversion and the BTEX yield exhibit a volcanic curve; i.e., they first increase and then decrease with the increase of mixed alkali concentration, among which HM-18 shows the highest tetralin conversion and BTEX yield, reaching 99.6% and 49.2%, respectively. However, the tetralin conversion and BTEX yield of HM-0.54 dramatically drop to 57.3% and 20.2%, respectively. The similar catalytic performance of HM-54, HM-18, and HM-9 indicates that the size of mesopores does not affect the catalytic performance significantly, considering the similar acid amounts of these catalysts (Table 1). The sharp decay of the catalytic performance for HM-0.675 and HM-0.54 can be attributed to their decreased acid amounts (Table 1) and fragmented structure (Figure 3f2, g2). In order to exclude the effects of acid amount, parent ZSM-5 with similar acid amount to HM-∞ and HM-18 was prepared (Figure S9), which was denoted as P-Z5*, and its catalytic activity is included in Figure 10a. Considering the similar acid amounts of P-Z5*, HM-∞, and HM-18, the creation of a hollow structure improves the catalytic activity, and the presence of mesopores further enhances the catalytic performance. Moreover, it is noticeable that the yields of meta-xylene (MX) and ortho-xylene (OX) for HM-18 are higher than those for P-Z5* and HM-∞, which indicates that the presence of mesopores promotes the diffusion of large molecules. Combined with the Py-IR results (Table 2), despite the fact that the B/L values of HM-18 and HM-0.54 are close, the conversion of tetralin and the yield of BTEX for HM-0.54 are much lower, which can be attributed to the collapse of the hollow mesoporous structure. The above results suggest that both the hollow mesoporous structure and the acid sites are important for the hydrocracking performance of the catalysts.

The yield of BTEX depends on both its selectivity and the liquid yield. Figure 10b illustrates the BTEX selectivity and the corresponding liquid yields of the catalysts. When the Si/Al ratio decreases from 61 for P-Z5 to 38 for P-Z5*, the BTEX selectivity increases from 42.9% to 70.1%, respectively. This indicates that the increase of acid amount promotes the BTEX selectivity. However, the liquid yield decreases with the increase of acid amount, suggesting that excess acidity causes serious side reactions, and more gas-phase products are produced through cracking. By contrast, the liquid yields of HM-54, HM-18, HM-9, and HM-1.35, which possess similar acidity with P-Z5*, are obviously improved compared to P-Z5*, indicating that the hollow mesoporous structure is more conducive to the production of liquid-phase products. Therefore, the hollow mesoporous catalysts exhibit an improved BTEX yield.

The long-term stabilities of P-Z5* and HM-18 were also evaluated, as shown in Figure 10c,d. As can be seen, the BTEX yield and the tetralin conversion of both P-Z5* and HM-18 first increase due to the induction period and then decrease. Under the same reaction conditions, the BTEX yield of P-Z5* sharply drops from 41.6% to 12.1%, and the tetralin conversion also rapidly declines from 94.1% to 54.2% after only 15 h. By contrast, the BTEX yield of HM-18 gradually decreases from 49.2% to 16.3% after 48 h, and the conversion of tetralin drops from 99.6% to 58.3%. This indicates that the lifetime of the catalyst is effectively prolonged through the construction of a hollow mesoporous structure.

The improved diffusion properties of hollow ZSM-5 and hollow mesoporous ZSM-5 compared to P-Z5 were proved by the IGA testing. As shown in Figure 11, the diffusion time

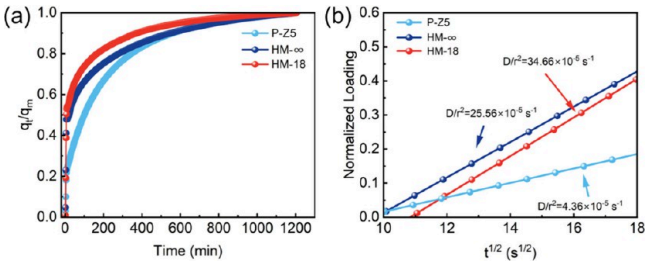

Figure 11. Adsorption kinetics curves of ortho-xylene on P-Z5, HM-∞, and HM-18: (a) ortho-xylene absorption curves of P-Z5, HM-∞, and HM-18, and (b) normalized amount of adsorption profiles in a short time domain.

constants are in the order of HM-18 (34.66×10^{-5} s^{-1}) > HM-∞ (25.56×10^{-5} s^{-1}) > P-Z5 (4.36×10^{-5} s^{-1}), consistent well with their catalytic activities. The above results demonstrate that the improved catalytic activity of hollow mesoporous ZSM-5 is closely related to the enhanced diffusion due to the generation of mesopores in the shell.

The deposited coke on the spent catalysts was investigated by TG analysis. The amount and rate of coke deposition on P-Z5, HM-∞, and HM-x were calculated, and the results are shown in Figure 12 and Table S4. From the TG curves shown

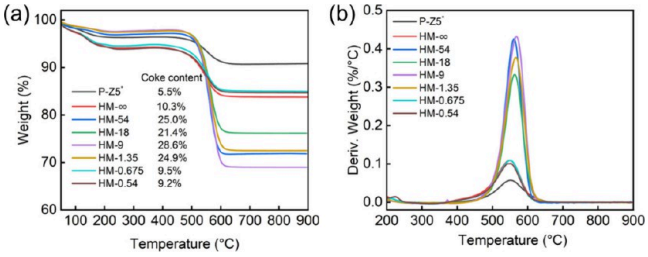

Figure 12. (a) TG and (b) DTG profiles of P-Z5*, HM-∞, and HM-x.

in Figure 12a, the weight loss below 250 °C is mainly due to the physically adsorbed water, tetralin, and aromatic products. The weight loss above 450 °C originates from the decomposition and combustion of coke species on the spent catalysts, based on which the amount of coke deposited on each catalyst was calculated. The three catalysts HM-54, HM-18, and HM-9, which exhibit better catalytic performance than HM-∞, have much higher coke amounts (21.4%−28.6%) compared to HM-∞ (10.3%). Since all these spent catalysts were obtained after a same reaction time of 27 h, the change trend of calculated coke deposition rate is consistent with that of the amount of coke. The above results indicate that the creation of hollow mesoporous structure improves the tolerance capacity for coke species, thus prolonging the lifetime of the catalysts. At the same time, there is a notable decrease in coke formation for HM-0.675 (9.5%) and HM-0.54 (9.2%), which can be explained by the decreased tetralin conversion, resulting from the diminished acid sites and structure fragmentation caused by the excess alkali etching.

https://doi.org/10.1021/acs.iecr.4c04323
Ind. Eng. Chem. Res. 2025, 64, 4330−4341

The differential thermogravimetric (DTG) curves in Figure 12b show that the temperatures corresponding to the maximum combustion rate of coke on each catalyst are almost the same, indicating that the substances constituting coke are similar.

4. CONCLUSIONS

In summary, we successfully synthesized hollow mesoporous ZSM-5 (HM-x) with homogeneous and tunable mesopores through a one-step mixed alkali treatment. The diameter of mesopores can be regulated in the range of 2−12 nm by controlling the concentration of Na_2CO_3 in the mixed alkali. The size of mesopores is also influenced by the alkali treatment duration, the Si/Al ratio of parent ZSM-5, and the zeolite/solution ratio. In the hydrocracking reaction of tetralin, the conversion of tetralin and the yield of BTEX for hollow mesoporous ZSM-5 exhibit obvious enhancement compared to those of parent ZSM-5 with a similar acid amount. Moreover, a long-term operation evaluation confirms the better stability and longer lifespan of hollow mesoporous ZSM-5. This improvement in catalytic performance can be attributed to the existence of mesopores within the ZSM-5 structure, which promotes the diffusion of large molecules, increases the accessibility to active sites, and enhances the tolerance capacity of coke species.

■ ASSOCIATED CONTENT

Supporting Information

The Supporting Information is available free of charge at https://pubs.acs.org/doi/10.1021/acs.iecr.4c04323.

TEM images; XRD patterns; SEM images; ^{27}Al MAS NMR spectra; EDS line scan profile; NH_3-TPD profiles; Relative crystallinity; Textural properties; Catalytic performance data; The amount and rate of coke deposition (PDF)

■ AUTHOR INFORMATION

Corresponding Authors

Keyan Li − *State Key Laboratory of Fine Chemicals, Frontiers Science Center for Smart Materials, PSU-DUT Joint Center for Energy Research, School of Chemical Engineering, Dalian University of Technology, Dalian 116024, China;* orcid.org/0000-0003-0467-6684; Email: keyanli@dlut.edu.cn

Xinwen Guo − *State Key Laboratory of Fine Chemicals, Frontiers Science Center for Smart Materials, PSU-DUT Joint Center for Energy Research, School of Chemical Engineering, Dalian University of Technology, Dalian 116024, China;* orcid.org/0000-0002-6597-4979; Email: guoxw@dlut.edu.cn

Authors

Haoqing Zhang − *State Key Laboratory of Fine Chemicals, Frontiers Science Center for Smart Materials, PSU-DUT Joint Center for Energy Research, School of Chemical Engineering, Dalian University of Technology, Dalian 116024, China*

Limin Zhang − *State Key Laboratory of Fine Chemicals, Frontiers Science Center for Smart Materials, PSU-DUT Joint Center for Energy Research, School of Chemical Engineering, Dalian University of Technology, Dalian 116024, China*

Mengdi Wang − *State Key Laboratory of Fine Chemicals, Frontiers Science Center for Smart Materials, PSU-DUT Joint Center for Energy Research, School of Chemical Engineering, Dalian University of Technology, Dalian 116024, China*

Anfeng Zhang − *State Key Laboratory of Fine Chemicals, Frontiers Science Center for Smart Materials, PSU-DUT Joint Center for Energy Research, School of Chemical Engineering, Dalian University of Technology, Dalian 116024, China;* orcid.org/0000-0002-4503-5755

Hao Wang − *State Key Laboratory of Fine Chemicals, Frontiers Science Center for Smart Materials, PSU-DUT Joint Center for Energy Research, School of Chemical Engineering, Dalian University of Technology, Dalian 116024, China*

Jiaming Wu − *State Key Laboratory of Fine Chemicals, Frontiers Science Center for Smart Materials, PSU-DUT Joint Center for Energy Research, School of Chemical Engineering, Dalian University of Technology, Dalian 116024, China*

Shanfan Lin − *National Engineering Research Center of Lower-Carbon Catalysis Technology, Dalian National Laboratory for Clean Energy, iChEM (Collaborative Innovation Center of Chemistry for Energy Materials), Dalian Institute of Chemical Physics, Chinese Academy of Sciences, Dalian 116023, China*

Duo Li − *State Key Laboratory of Fine Chemicals, Frontiers Science Center for Smart Materials, PSU-DUT Joint Center for Energy Research, School of Chemical Engineering, Dalian University of Technology, Dalian 116024, China*

Chunshan Song − *State Key Laboratory of Fine Chemicals, Frontiers Science Center for Smart Materials, PSU-DUT Joint Center for Energy Research, School of Chemical Engineering, Dalian University of Technology, Dalian 116024, China; Department of Chemistry, Faculty of Science, The Chinese University of Hong Kong, Shatin, Hong Kong 999077, China;* orcid.org/0000-0003-2344-9911

Complete contact information is available at: https://pubs.acs.org/10.1021/acs.iecr.4c04323

Author Contributions

‖H. Zhang and L. Zhang contributed equally to this work.

Notes

The authors declare no competing financial interest.

■ ACKNOWLEDGMENTS

This work was financially supported by the National Key R&D Program of China (2022YFA1503400).

■ REFERENCES

(1) Jin, T.; Xia, D. H.; Xiang, Y. Z.; Zhou, Y. L. The Effect of Metal Introduced Over ZSM-5 Zeolite for C_9 Heavy Aromatics Hydrodealkylation. *Pet. Sci. Technol.* **2009**, *27* (16), 1821−1835.

(2) Saeedi, M.; Li, L. Y.; Salmanzadeh, M. Heavy metals and polycyclic aromatic hydrocarbons: pollution and ecological risk assessment in street dust of Tehran. *J. Hazard. Mater.* **2012**, *227*, 9−17.

(3) Kasipandi, S.; Bae, J. W. Recent Advances in Direct Synthesis of Value Added Aromatic Chemicals from Syngas by Cascade Reactions over Bifunctional Catalysts. *Adv. Mater.* **2019**, *31* (34), 1803390.

(4) Saab, R.; Polychronopoulou, K.; Zheng, L. X.; Kumar, S.; Schiffer, A. Synthesis and performance evaluation of hydrocracking catalysts: A review. *J. Ind. Eng. Chem.* **2020**, *89*, 83−103.

(5) Kostyniuk, A.; Bajec, D.; Likozar, B. Catalytic hydrocracking reactions of tetralin biomass tar model compound to benzene, toluene and xylenes (BTX) over metal-modified ZSM-5 in ambient pressure reactor. *Renewable Energy* **2022**, *188*, 240−255.
(6) Chen, F.; Zhang, G. H.; Weng, X. Y.; Zhang, Y. H.; Zhao, L.; Cao, L. Y.; Gao, J. S.; Xu, C. M.; Liu, X. Q.; Gao, X. H. High value utilization of inferior diesel for BTX production: Mechanisms, catalysts, conditions and challenges. *Appl. Catal., A* **2021**, *616*, 118095.
(7) Dang, H.; Chen, S. L.; Wu, Z. J.; Wang, L.; Zhang, Y. T. Effect of Zn Contents of W/Zn-Beta Catalysts on Their Catalytic Performance in the Selective Hydrocracking of Tetrahydronaphthalene into Benzene, Toluene, and Xylene. *Energy Fuels* **2023**, *37* (12), 8486−8499.
(8) Wang, Q.; Hou, Z. G.; Zhang, B.; Liu, J.; Song, W. Y.; Xue, D. S.; Liu, L. Z.; Wang, D.; Chen, X. G. Preparation of a highly efficient Pt/USY catalyst for hydrogenation and selective ring-opening reaction of tetralin. *Petroleum Science* **2018**, *15* (3), 605−612.
(9) Cao, Z. B.; Xu, X. L.; Qi, Y. T.; Lu, S. W.; Qi, B. F. Hydrocracking of tetralin over Mo-Ni/USY dual functional catalysts. *Pet. Sci. Technol.* **2004**, *22* (5−6), 617−629.
(10) Kostyniuk, A.; Bajec, D.; Likozar, B. Catalytic hydrocracking reactions of tetralin as aromatic biomass tar model compound to benzene/toluene/xylenes (BTX) over zeolites under ambient pressure conditions. *J. Ind. Eng. Chem.* **2021**, *96*, 130−143.
(11) Chen, Y. Y.; Wu, H. B.; Wang, S.; Shi, D. Z.; Dong, M.; Qin, Z. F.; Wang, J. G.; Fan, W. B. Reaction mechanism of co-coupling conversion of propane and methanol over H-ZSM-5 zeolite. *J. Catal.* **2023**, *425*, 260−268.
(12) Timoshev, V.; Haufe, L. A.; Seifert, M.; Busse, O.; Wu, Y. F.; Wiegand, T.; Weigand, J. J. Enhancing Hydrothermal Stability of ZSM-5 Cracking Additives with Aluminum Phosphates. *Ind. Eng. Chem. Res.* **2024**, *63*, 11800−11814.
(13) Guo, D. R.; Zhu, M. H.; Yang, Z. X.; Han, Y. F. Insights into Catalytic Cracking of n-Heptane over Ga-Doped Hierarchical ZSM-5. *Ind. Eng. Chem. Res.* **2024**, *63* (25), 10965−10980.
(14) Wang, N.; Sun, Q. M.; Zhang, T. J.; Mayoral, A.; Li, L.; Zhou, X.; Xu, J.; Zhang, P.; Yu, J. H. Impregnating Subnanometer Metallic Nanocatalysts into Self-Pillared Zeolite Nanosheets. *J. Am. Chem. Soc.* **2021**, *143* (18), 6905−6914.
(15) Shi, J.; Wang, Y. D.; Yang, W. M.; Tang, Y.; Xie, Z. K. Recent advances of pore system construction in zeolite-catalyzed chemical industry processes. *Chem. Soc. Rev.* **2015**, *44* (24), 8877−8903.
(16) Zhang, H. T.; Xi, Z. X.; Wang, H. Y.; Zhang, J. X.; Zhou, A. J.; Xu, R. W.; Zhang, A. F.; Guo, X. W. High Stability Catalyst for Butene Cracking with Ultrathin ZSM-5 Nanoplates. *Ind. Eng. Chem. Res.* **2024**, *63* (36), 15637−15645.
(17) Wei, Y.; Feng, J.; Guan, B.; Yu, J. Structural Engineering of Hierarchical Zeolite-Based Catalysts. *Acc. Mater. Res.* **2024**, *5* (7), 857−871.
(18) Ji, Y.; Yang, H.; Yan, W. Strategies to Enhance the Catalytic Performance of ZSM-5 Zeolite in Hydrocarbon Cracking: A Review. *Catalysts* **2017**, *7* (12), 367−398.
(19) Fu, T.; Qi, R.; Wang, X.; Wan, W.; Li, Z. Facile synthesis of nano-sized hollow ZSM-5 zeolites with rich mesopores in shell. *Microporous Mesoporous Mater.* **2017**, *250*, 43−46.
(20) Xu, Y.; Wang, J.; Ma, G.; Lin, J.; Ding, M. Designing of Hollow ZSM-5 with Controlled Mesopore Sizes to Boost Gasoline Production from Syngas. *ACS Sustainable Chem. Eng.* **2019**, *7* (21), 18125−18132.
(21) Liu, X.; Shi, J.; Yang, G.; Zhou, J.; Wang, C.; Teng, J.; Wang, Y.; Xie, Z. A diffusion anisotropy descriptor links morphology effects of H-ZSM-5 zeolites to their catalytic cracking performance. *Commun. Chem.* **2021**, *4* (1), 107.
(22) Kim, T.; Kim, G. P.; Jang, J.; Shim, S. E.; Ahn, W. S.; Baeck, S. H. An investigation on the selective hydrodealkylation of C_{9+} aromatics over alkali-treated Pt/H-ZSM-5 zeolites. *Catal. Sci. Technol.* **2016**, *6* (14), 5599−5607.
(23) Groen, J. C.; Zhu, W. D.; Brouwer, S.; Huynink, S. J.; Kapteijn, F.; Moulijn, J. A.; Pérez-Ramírez, J. Direct demonstration of enhanced diffusion in mesoporous ZSM-5 zeolite obtained via controlled desilication. *J. Am. Chem. Soc.* **2007**, *129* (2), 355−360.
(24) Dai, C. Y.; Zhang, A. F.; Liu, M.; Guo, X. W.; Song, C. S. Hollow ZSM-5 with Silicon-Rich Surface, Double Shells, and Functionalized Interior with Metallic Nanoparticles and Carbon Nanotubes. *Adv. Funct. Mater.* **2015**, *25* (48), 7479−7487.
(25) Ma, Z.; Fu, T. J.; Wang, Y. J.; Shao, J.; Ma, Q.; Zhang, C. M.; Cui, L. P.; Li, Z. Silicalite-1 Derivational Desilication-Recrystallization to Prepare Hollow Nano-ZSM-5 and Highly Mesoporous Micro-ZSM-5 Catalyst for Methanol to Hydrocarbons. *Ind. Eng. Chem. Res.* **2019**, *58* (6), 2146−2158.
(26) Fu, T.; Qi, R.; Wan, W.; Shao, J.; Wen, J. Z.; Li, Z. Fabrication of Hollow Mesoporous Nanosized ZSM-5 Catalyst with Superior Methanol to Hydrocarbons Performance by Controllable Desilication. *ChemCatChem.* **2017**, *9* (22), 4212−4224.
(27) Ning, W. W.; Yang, X. N.; Zheng, J. J.; Sun, X. B.; Pan, M.; Li, R. F. An environmentally friendly route to prepare hierarchical ZSM-12 using waste liquor as partial nutrients. *Mater. Chem. Phys.* **2019**, *223*, 299−305.
(28) Qin, Y. C.; Gao, X. H.; Zhang, H. T.; Zhang, S. H.; Zheng, L. G.; Li, Q.; Mo, Z. S.; Duan, L. H.; Zhang, X. T.; Song, L. J. Measurements and distinguishment of mass transfer processes in fluid catalytic cracking catalyst particles by uptake and frequency response methods. *Catal. Today* **2015**, *245*, 147−154.
(29) Bensafi, B.; Chouat, N.; Djafri, F. The universal zeolite ZSM-5: Structure and synthesis strategies. A review. *Coord. Chem. Rev.* **2023**, *496*, 215397.
(30) Silaghi, M. C.; Chizallet, C.; Raybaud, P. Challenges on molecular aspects of dealumination and desilication of zeolites. *Microporous Mesoporous Mater.* **2014**, *191*, 82−96.
(31) Li, J. J.; Liu, M.; Guo, X. W.; Zeng, S.; Xu, S. T.; Wei, Y. X.; Liu, Z. M.; Song, C. S. Influence of Al Coordinates on Hierarchical Structure and T Atoms Redistribution during Base Leaching of ZSM-5. *Ind. Eng. Chem. Res.* **2018**, *57* (45), 15375−15384.
(32) Sun, Z.; Shu, Q.; Zhang, Q.; Li, S.; Zhu, G.; Wang, C.; Zhang, J.; Li, H.; Huang, Z. A Hydrothermal Synthesis Process of ZSM-5 Zeolite for VOCs Adsorption Using Desilication Solution. *Separations* **2024**, *11* (2), 39.
(33) Zhang, C. D.; Kwak, G.; Park, H. G.; Jun, K. W.; Lee, Y. J.; Kang, S. C.; Kim, S. Light hydrocarbons to BTEX aromatics over hierarchical HZSM-5: Effects of alkali treatment on catalytic performance. *Microporous Mesoporous Mater.* **2019**, *276*, 292−301.
(34) Zhang, C.; Kwak, G.; Lee, Y. J.; Jun, K. W.; Gao, R.; Park, H. G.; Kim, S.; Min, J. E.; Kang, S. C.; Guan, G. F. Light hydrocarbons to BTEX aromatics over Zn-modified hierarchical ZSM-5 combined with enhanced catalytic activity and stability. *Microporous Mesoporous Mater.* **2019**, *284*, 316−326.
(35) Fu, T. J.; Wang, Y. J.; Li, Z. Surface-Protection-Induced Controllable Restructuring of Pores and Acid Sites of the Nano-ZSM-5 Catalyst and Its Influence on the Catalytic Conversion of Methanol to Hydrocarbons. *Langmuir.* **2020**, *36* (14), 3737−3749.
(36) Sazama, P.; Wichterlova, B.; Dedecek, J.; Tvaruzkova, Z.; Musilova, Z.; Palumbo, L.; Sklenak, S.; Gonsiorova, O. FTIR and ^{27}Al MAS NMR analysis of the effect of framework Al- and Si-defects in micro- and micro-mesoporous H-ZSM-5 on conversion of methanol to hydrocarbons. *Microporous Mesoporous Mater.* **2011**, *143* (1), 87−96.
(37) Wang, S.; Wang, P. F.; Qin, Z. F.; Chen, Y. Y.; Dong, M.; Li, J. F.; Zhang, K.; Liu, P.; Wang, J. G.; Fan, W. B. Relation of Catalytic Performance to the Aluminum Siting of Acidic Zeolites in the Conversion of Methanol to Olefins, Viewed via a Comparison between ZSM-5 and ZSM-11. *ACS Catal.* **2018**, *8* (6), 5485−5505.
(38) Dai, C. Y.; Zhang, A. F.; Li, L. L.; Hou, K. K.; Ding, F. S.; Li, J.; Mu, D. Y.; Song, C. S.; Liu, M.; Guo, X. W. Synthesis of Hollow Nanocubes and Macroporous Monoliths of Silicalite-1 by Alkaline Treatment. *Chem. Mater.* **2013**, *25* (21), 4197−4205.

https://doi.org/10.1021/acs.iecr.4c04323
Ind. Eng. Chem. Res. 2025, 64, 4330−4341

(39) Fodor, D.; Pacosova, L.; Krumeich, F.; van Bokhoven, J. A. Facile synthesis of nano-sized hollow single crystal zeolites under mild conditions. *Chem. Commun.* **2014**, *50* (1), 76−78.
(40) Li, J. J.; Chen, H. H.; Liu, W.; Zhi, Y. C.; Ta, N.; Xie, S. J.; Xu, L. Y.; Li, X. J.; Zhu, X. X.; Xu, S. T. Unravelling the Crucial of Spatial Al Distribution to Realize Precise Alkali-Treatment for Target Acid-Catalyzed Reactions. *Angew. Chem., Int. Ed.* **2025**, *64*, e202416564.
(41) Pérez-Ramírez, J.; Verboekend, D.; Bonilla, A.; Abelló, S. Zeolite Catalysts with Tunable Hierarchy Factor by Pore-Growth Moderators. *Adv. Funct. Mater.* **2009**, *19* (24), 3972−3979.
(42) Wan, W.; Fu, T.; Qi, R.; Shao, J.; Li, Z. Coeffect of Na^+ and Tetrapropylammonium (TPA^+) in Alkali Treatment on the Fabrication of Mesoporous ZSM-5 Catalyst for Methanol-to-Hydrocarbons Reactions. *Ind. Eng. Chem. Res.* **2016**, *55* (51), 13040−13049.

https://doi.org/10.1021/acs.iecr.4c04323
Ind. Eng. Chem. Res. 2025, 64, 4330−4341